

# Event3DGS: Event-based 3D Gaussian Splatting for Fast Egomotion

Tianyi Xiong<sup>\*1</sup> Jiayi Wu<sup>\*1</sup> Botao He<sup>1</sup> Cornelia Fermuller<sup>1</sup>  
 Yiannis Aloimonos<sup>1</sup> Heng Huang<sup>1</sup> Christopher A. Metzler<sup>1</sup>

<sup>1</sup>University of Maryland, College Park

## Abstract:

The recent emergence of 3D Gaussian splatting (3DGS) leverages the advantage of explicit point-based representations, which significantly improves the rendering speed and quality of novel-view synthesis. However, 3D radiance field rendering in environments with high-dynamic motion or challenging illumination condition remains problematic in real-world robotic tasks. The reason is that fast egomotion is prevalent real-world robotic tasks, which induces motion blur, leading to inaccuracies and artifacts in the reconstructed structure. To alleviate this problem, we propose Event3DGS, the first method that learns Gaussian Splatting solely from raw event streams. By exploiting the high temporal resolution of event cameras and explicit point-based representation, Event3DGS can reconstruct high-fidelity 3D structures solely from the event streams under fast egomotion. Our sparsity-aware sampling and progressive training approaches allow for better reconstruction quality and consistency. To further enhance the fidelity of appearance, we explicitly incorporate the motion blur formation process into a differentiable rasterizer, which is used with a limited set of blurred RGB images to refine the appearance. Extensive experiments on multiple datasets validate the superior rendering quality of Event3DGS compared with existing approaches, with over 95% lower training time and faster rendering speed in orders of magnitude.

**Keywords:** Event-based 3D Reconstruction, Gaussian Splatting, Fast Egomotion

## 1 Introduction

Reconstructing accurate and visually realistic 3D scenes from 2D images taken from various viewpoints has long been a challenge in computer vision and graphics. In recent developments, significant strides have been made in advancing this endeavor through two notable contributions: Neural Radiance Fields (NeRF) [1] and 3D Gaussian Splatting (3DGS) [2]. Both categories of methods represent scenes as differentiable, continuous 3D representations, enabling the rendering from new views to exhibit visual fidelity comparable to evaluation images. However, the efficacy of radiance field rendering is substantially influenced by on the quality of input images. Fast egomotion, which is common in real-world robotic tasks, can induce motion blur artifacts within rendered images, thereby compromising visual fidelity and realism, hindering the neural rendering methods' (such as NeRF and 3DGS) practical applicability in real-world scenes. Although recent studies [3, 4, 5, 6, 7, 8] have



Figure 1: Event3DGS can reconstruct structure and color details using only event-streams.

However, the efficacy of radiance field rendering is substantially influenced by on the quality of input images. Fast egomotion, which is common in real-world robotic tasks, can induce motion blur artifacts within rendered images, thereby compromising visual fidelity and realism, hindering the neural rendering methods' (such as NeRF and 3DGS) practical applicability in real-world scenes. Although recent studies [3, 4, 5, 6, 7, 8] have

<sup>\*</sup>Indicates equal contribution.

demonstrated promising advancements in reconstructing radiance fields from motion-blurred images by adding the capability to infer camera motion during the exposure period, they are inherently constrained by the presence of motion ambiguities and the inevitable loss of sharp geometry details, which remain unrecoverable solely from the blurry image data.

The event camera, a novel sensing paradigm, offers several advantages over frame-based cameras, particularly in scenarios characterized by fast egomotion. By asynchronously recording pixel-level illumination change, it can achieve microsecond-level temporal resolution, does not suffer from motion blur, and has a much higher dynamic range than standard cameras. Such attributes empower event cameras to furnish a continuous flow of pixel-level intensity variations and precise and sharp scene geometry information, even in fast egomotion scenarios [9]. Within radiance field rendering, the inherent capability of event cameras to precisely capture scene information at high temporal resolutions seamlessly aligns with the demands posed by radiance field rendering in fast egomotion scenarios. Employing a continuous event stream, characterized by sharp scene geometry, as a supervisory signal for radiance field rendering, holds promise in facilitating the generation of coherent and artifact-free renderings for rapid egomotion situations.

We propose Event3DGS (see Fig.1), the first method that leverages the advantages of gaussian splatting to facilitate high-fidelity 3D reconstruction and real time rendering based solely on event data. Event3DGS is trained from events by comparing the approximate difference of accumulated observed events between views against the difference between the rendering views. Our findings demonstrate the feasibility of rendering the accurate geometry of the scene using 3DGS solely from an event stream input. Our method effectively utilizes event and optional blurred image data, enabling explicit 3D scene representation recovery during rapid egomotion. Extensive experiments in both simulation and real-world validate that our method can generate comparable and often more visually appealing rendering quality than prevailing pipeline approaches, while achieving faster rendering speed at lower data bandwidth. Our contributions can be summarized as follows:

1. To the best of our knowledge, this is the first work to produce explicit 3D Gaussian splatting scene representations solely from event data.
2. With the proposed neutralization & sparsity-aware sampling and differential supervision approaches tailored to adapting 3DGS to event data, more accurate 3D geometry reconstruction and faster real-time rendering functionalities are achieved.
3. By incorporating the motion blur formation process into a differentiable rasterizer and utilizing a subset of blurry RGB images, better appearance fidelity in the rendered scene is achieved compared with baseline methods.

## 2 Background and Related Work

### 2.1 Novel View Synthesis and 3D Gaussian Splattings

3D scene reconstruction and novel-view synthesis is a fundamental task in graphics and computer vision [1, 10, 11, 12], boosting applications in autonomous driving [13], robotics [14] and virtual reality [15]. NeRF [1] and its variants [16, 17, 18, 19, 20, 21] model a scene implicitly with an MLP-based neural network and utilize differentiable volume rendering, achieving state-of-the-art rendering results with high fidelity and fine details. However, since a large number of points need to be sampled to accumulate the color of each pixel, these methods suffer from low rendering efficiency and long training time. Extended works on radiance fields work by interpolating values from explicit density representations such as points[22], voxel grids [23, 24, 25], or hash grids[26]. Although these methods achieve higher efficiency than the vanilla MLP version, they still need multiple queries for each pixel, lacking real-time rendering capacity.

In light of these challenges, recent research has explored alternative 3D representations for better efficiency and visual fidelity. 3D Gaussian Splatting (3DGS) [2] employed a set of optimized Gaussian splats to achieve state-of-the-art reconstruction quality and rendering speed. Initialized from sparse SfM pointclouds, 3DGS is trained via differentiable rendering to adaptively control the density and refine the shape and appearance parameters. A tiled-based rasterizer was proposed to allow

for real-time rendering. 3DGS has very high accuracy and speed, and multiple works have applied the technique in applications such as SLAM [27, 28], dynamic reconstruction [29, 30], and scene editing [31, 32]. However, all these methods require RGB images as input.

## 2.2 Event-based 3D Reconstruction and Radiance Field Rendering

Event-based and event-aided 3D reconstruction [33, 34, 35, 36, 37, 38, 39, 40] and radiance field rendering [41, 42, 43, 44, 45, 46] represent a paradigm shift in computer vision and graphics, enhancing the perception of dynamic scenes with high temporal resolution and accuracy. Weikersdorfer et al. [47] demonstrated event-based stereo reconstruction, illustrating the potential for reconstructing 3D scenes using data from stereo event cameras. However, stereo matching can be challenging due to the sparse nature of event camera data, which often leads to unstable performance in depth estimation. Muglikar et al. [34] enhanced depth sensing by integrating an event camera with a laser projector. While this approach achieves better depth accuracy, the inclusion of a laser projector complicates its effectiveness in outdoor environments with challenging illumination conditions. Previous works introducing event-based radiance fields include Ev-NeRF [41], EventNeRF [42], and E-NeRF [48]. These approaches leverage the inherent multi-view consistency of NeRFs [1], providing a robust self-supervision signal for extracting coherent scene structures from raw event data. However, they inherit NeRF’s high computational complexity and challenges in real-time rendering. Additionally, NeRF’s implicit representation complicates editing and integration with traditional 3D graphics processing pipelines.

Our proposed Event3DGS offers real-time, explicit, interpretable scene geometry depiction and editable high-fidelity 3D rendering. It allows seamless integration with established graphics pipelines and enables streamlined optimization. Event3DGS is robust under agile motion, low light, and high dynamic range scenarios where RGB cameras fail to deliver. By combining the event camera’s hardware advantages with 3DGS’s efficient rendering, our pipeline enables real-time 3D rendering of diverse scenes with low latency, low data bandwidth, and ultra-low power consumption, which supports 3D mapping at a higher operating speed.

## 3 Methodology

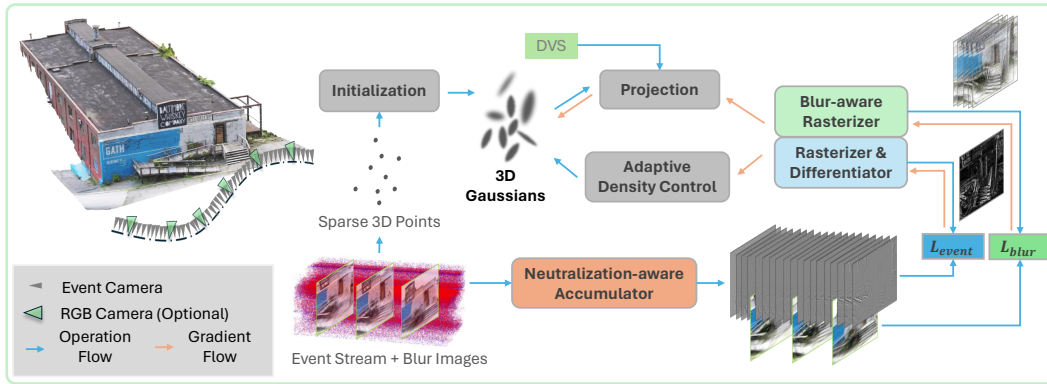


Figure 2: **Event3DGS model architecture.** We first utilize a neutralization-aware accumulator and sparsity-aware sampling strategy to slice the input event stream into frames. Then, each sampled event frame is utilized to supervise the difference between two rendered views, optimizing the 3D Gaussians to reconstruct sharp geometric structures from high-speed egomotion. We further leverage progressive training to better reconstruct scene details. Optionally, we integrate a few motion-blurred RGB images from an attached camera into the pipeline. We embed motion blur information into the rasterizer and use a parameter-separable alternating optimization strategy to calibrate the colorization while preserving geometric details.

The proposed Event3DGS aims to efficiently reconstruct a 3D scene representation from a given sequence of events (either grayscale or color) under fast egomotion and low-light conditions. Fig. 2 illustrates the overall architecture of the proposed Event3DGS. Unlike image-based reconstruction, our Event3DGS approach does not directly supervise the absolute radiance of rendered images

during optimization. Instead, we integrate the event formation process into the 3DGS pipeline and utilize the observed events as ground truth to implement differential self-supervision within the gradient-based optimization framework. In addition, in order to solve the scale ambiguity problem of radiance inherent in event data, we describe a parametrically separable fine-tuning approach for appearance refinement, aligning geometrically sharp 3DGS reconstructed from events with true scene radiance and texture details using a small number of free blurred views.

### 3.1 Preliminary

3D Gaussian Splatting (3DGS) [2] explicitly represents a scene with a set of anisotropic 3D Gaussians (ellipsoids). Each Gaussian is defined by a full 3D covariance matrix  $\Sigma$  with its center point (mean)  $\mu$ :

$$G(x) = e^{-\frac{1}{2}x^T \Sigma^{-1} x} \quad (1)$$

To preserve the valid positive semi-definite property during optimization, the covariance matrix is decomposed into  $\Sigma = RSS^T R^T$ , where  $S \in \mathbb{R}_+^k$  represents scaling factors and  $R \in SE(3)$  is the rotation matrix. Each Gaussian is also described with an opacity factor  $\sigma \in \mathbb{R}$ , and spherical harmonics  $\mathcal{C} \in \mathbb{R}^k$  for modeling view-dependent effects.

During optimization, 3D Gaussian splatting adaptively controls Gaussian density via densification in areas with large view-space positional gradients and pruning points with low opacity. For rendering, the 3D Gaussians  $G(x)$  are first projected onto the 2D imaging plane  $G'(x)$ , then a tile-based rasterizer is proposed to enable fast sorting and  $\alpha$ -blending. The color of pixel  $u$  is calculated via blending  $N$  ordered overlapping points:

$$C(u) = \sum_{i=1}^N c_i \alpha_i \prod_{j=1}^{i-1} (1 - \alpha_j) \quad (2)$$

where  $c_i = f(\mathcal{C}_i)$  is the color modeled via spherical harmonics, and  $\alpha_i = \sigma_i G'_i(u)$  is the multiplication of opacity and the transformed 2D Gaussian.

### 3.2 Neutralization-aware Slicing & Sparsity-aware Sampling

The input to our Event3DGS pipeline comprises a continuous stream of events  $\mathbf{e} = (t, \mathbf{u}, p)$ , each indicating a detected increase or decrease in logarithmic brightness (denoted by the polarity  $p \in (-1, 1)$ ) at a specific time instant  $t$  and pixel location  $\mathbf{u} = (x, y)$ . In order to efficiently utilize event data, a common practice is to use event windows to accumulate corresponding events, which requires us to slice the event stream. In event-based radiance field rendering pipelines, the slicing strategy of the event stream affects rendering quality of the scene. This impact is particularly notable within our pipeline, as neutralization is inevitable during the accumulation of polarity. Notably, existing works[42, 49] have shown that using constant short windows leads to poor propagation of high-level illumination, and using constant long windows often leads to poor local detail. To mitigate the information loss, we design a neutralization-aware event slicing strategy. Our slicing strategy considers the number of events and the neutralization moment to adaptively sample the length of the event integration window. (1) perform slicing when the number of events reaches the threshold; (2) perform slicing where neutralization occurs on many pixels (set threshold manually). This not only ensures the diversity of window lengths but also minimizes the loss of detailed information caused by neutralization.

Uniform radiance regions typically do not trigger events, resulting in spatial sparsity of event data as supervision signals. To mitigate this issue, we introduce low-level gaussian noise  $\mathcal{N}(\mu_{noevt}, \sigma_{noevt}^2)$  during the sampling process to augment pixels that no events throughout the entire event window, which enhances the gradient-based optimization on uniform radiance regions and make our pipeline more robust to noise events. The mathematical details is shown in Eq. 3:

$$\mathbf{E}_{\mathbf{u}}(\mathbf{t}_s, \mathbf{t}_e) = \begin{cases} \int_{t_s}^{t_e} \Delta e_{\mathbf{u}}(\tau) d\tau & \text{if \# of event triggers} \neq 0 \\ \Delta \cdot \mathcal{N}(0, \sigma_{noevt}^2) & \text{if \# of event triggers} = 0 \end{cases} \quad (3)$$

where  $\mathbf{E}_{\mathbf{u}}$  denotes the accumulation of all event polarities triggered at pixel coordinate  $\mathbf{u}$  within the current event window,  $\sigma_{noevt} = 0.1$  in our experiments,  $t_s$  and  $t_e$  are the timestamps of the window start and the window end, respectively.

### 3.3 Event Rendering Loss integrating Structural Dissimilarity

Event data with high temporal resolution can provide supervision signals with sharp scene structure, allowing 3D gaussian splatting (3DGS) to perform fine-grained reconstruction of scene structure under fast egomotion. The multi-view consistency of event sequence guarantee the learnable Gaussians to continuously converge to the ground truth geometric structure and logarithmic color field of the scene during optimization. Our event rendering loss  $\mathcal{L}_{event}(t_s, t_e)$  compares the recorded events with the differential signal generated by adjacent view renderings according to the event formation model. Following [2], it primarily comprises two components: the  $\mathcal{L}_1$  loss, which measures the absolute log-radiance change difference at each pixel, and the structural dissimilarity loss  $\mathcal{L}_{DSSIM}$  [50], which accounts for the structural information between adjacent pixels. We define them as follows:

$$\mathcal{L}_1(t_s, t_e) = \left\| \frac{\mathbf{F} \odot (\log \tilde{\mathbf{C}}(t_e) - \log \tilde{\mathbf{C}}(t_s))}{g} - \mathbf{F} \odot \mathbf{E}(t_s, t_e) \right\|_1 \quad (4)$$

$$\mathcal{L}_{DSSIM}(t_s, t_e) = DSSIM\left(\frac{\mathbf{F} \odot (\log \tilde{\mathbf{C}}(t_e) - \log \tilde{\mathbf{C}}(t_s))}{g}, \mathbf{F} \odot \mathbf{E}(t_s, t_e)\right) \quad (5)$$

where  $\tilde{\mathbf{C}}(t)$  denotes the 2D rendering under the view at time  $t$ ,  $g$  is a gamma correction value initialized to 2.2 in our experiments which can be adjust in appearance refinement stage (see Sec. 3.5),  $\mathbf{E}$  represents the accumulation of all event polarities triggered within the field of view (FOV),  $\mathbf{F}$  is the RGGB Bayer filter [42], which only apply for colour events. The total loss can be written as, we set  $\lambda_{DSSIM}$  to 0.2 in our experiments:

$$\mathcal{L}_{event} = (1 - \lambda_{DSSIM})\mathcal{L}_1 + \lambda_{DSSIM}\mathcal{L}_{DSSIM} \quad (6)$$

### 3.4 Progressive Training

The quality of point cloud initialization greatly affects the reconstruction accuracy of Gaussian Splatting[2, 51]. With accurate positions, more fine-grained structural details structures can be acquired via the densification and splitting of large gaussians during training. As event-based SfM pipelines lacks accuracy, we find out that the pretrained Event3DGS checkpoint itself can serves as good initialization combined with low-density noises. Therefore, we can apply an opacity threshold  $\alpha_{pro}$  to filter the dense gaussians. The color and position factors of the selected gaussians serve as the initialization for the next-round training. We train Event3DGS in a progressive manner to gradually achieve better representation with structural details.

### 3.5 Blur-aware Rasterization and Parameter Separable Apperance Refinement

Although severely motion-blurred RGB images are challenging for radiance field training due to structural degradation, their true radiance scale and texture information complement event data. In this section, we aim to refine the appearance of Event3DGS via training on a small amount of motion blurred inputs, to improve visual fidelity while maintaining sharp scene structure.

In the realm of physics, camera motion blur stems from the amalgamation of radiance induced by the movement of the camera. According to the physical image formation, camera motion blur is produced by the integration of radiance during camera movement, which can be mathematically represented as following equation:

$$\mathbf{I}_{blur} = \int_{\tau_s}^{\tau_e} \mathbf{I}(\mathbf{P}_\tau) d\tau \approx \frac{1}{N} \sum_{i=1}^N \mathbf{I}(\mathbf{P}_{\tau_i}) \quad (7)$$

where  $\mathbf{I}_{blur}$  represents blurry image,  $\mathbf{I}(\mathbf{P}_\tau)$  is latent sharp image captured from the camera pose  $\mathbf{P}_\tau \in SE(3)$ . To simplify the integral calculation, we approximate it as a finite sum of  $N$  radiance  $\mathbf{I}(\mathbf{P}_{\tau_i})$ , where  $\tau_i$  are the midpoint timestamps of a finite number of event integration windows (EIW) within the exposure interval (from  $\tau_s$  to  $\tau_e$ ). To incorporate motion effects of camera movement during frame capturing into the differentiable rasterization process, we incorporate the above physical formation process of motion blur into the rendering equation:

$$\tilde{\mathbf{C}}_{blur}(x, y, \mathbf{P}_{\frac{\tau_s + \tau_e}{2}}, \mathcal{G}) = \frac{1}{N_{EIW}} \sum_{i=1}^{N_{EIW}} \tilde{\mathbf{C}}(x, y, \mathbf{P}_{\tau_i}, \mathcal{G}) \quad (8)$$



where  $\tilde{C}_{blur}$  denotes the blurry color of the pixel(x,y) of output image given by blur-aware volumetric rendering,  $\mathcal{G}$  is the 3D Gaussian model parameters,  $N_{EIW}$  represents the number of event integration windows within the exposure interval. The loss function  $\mathcal{L}_{blur}$  can be written as:

$$\mathcal{L}_{blur} = (1 - \lambda_{DSSIM}) \left\| \tilde{\mathbf{C}}_{\text{blur}} - \mathbf{I}_{\text{blur}} \right\|_1 + \lambda_{DSSIM} DSSIM(\tilde{\mathbf{C}}_{\text{blur}}, \mathbf{I}_{\text{blur}}) \quad (9)$$

To improve the fidelity of scene appearance from a few blurry RGB images while preserving sharp structural details from event sequences, we apply parameters separable optimization. We divide the learnable parameters into two groups. The structure-related parameters include the position  $\mu$ , scaling factor  $S$  and rotation factor  $R$ , and the appearance-related parameters include opacity  $\alpha$  and spherical harmonics (SH) coefficients. When trained on event streams, all parameters of Event3DGS are optimized to learn the structure and the approximate logarithmic color field of the target scene. After the parameters converge on the event-stream, we fix the structure-related parameters and only calculate gradients on the appearance-related parameters to refine the appearance component of the scene. We apply an extra scaling factor  $\eta_\alpha = 0.05$  onto the learning rate of opacity  $\alpha$  to inhibit drastic changes in density.

## 4 Experiments

**Synthetic and Real World Datasets** We evaluate our method using both synthetic and real data. For fair comparison, we adopt the synthetic dataset proposed in [42], which generates 7 sequences with 360° camera rotations around each 3D object, simulating event streams from 1000 views. For real-world datasets, we capture 5 colorful event sequences together with ground truth RGB images that include both indoor and outdoor scenes. We also evaluate the low-light performance on real sequences in [42], which are captured on a spinning table with a 5W light source.

**Metrics and Settings** We report three popular metrics to evaluate our methods: Peak Signal-to-Noise Ratio (PSNR) [52], Structural Similarity Index Measure (SSIM) [50], and AlexNet-based Learned Perceptual Patch Similarity (LPIPS) [53]. Following [42], we apply linear transformation in the logarithmic space for all our and baseline results. Our implementation is based on the official 3DGS[2] framework. We train our model on a single NVIDIA RTX6000Ada GPU for 30k iterations, and filter out the points with opacity threshold  $\alpha = 0.9$  for progressive training. We randomly initialize the point cloud according to scale of each training scene, and set the other hyperparameters and optimizer as default. For blur-aware

**Baselines** We benchmark our work against a NeRF-based method, EventNeRF[42], and a naive baseline E2VID[54] + NeRF[1], which cascades the event-to-video method E2VID to a vanilla 3DGS. For EventNeRF, we directly render rgb and depth images from the official pretrained weights for synthetic and low-light scenes. For real-world sequences, we train EventNeRF for 500k iterations under their default settings, and sweep across multiple event-window sizes to report the best results.

### 4.1 Quantitative Evaluation

**Synthetic Sequences** Table 1 demonstrates that our Event3DGS method consistently outperforms both baselines across almost all synthetic scenes in all metrics. On average, our method achieves a +2.61dB higher PSNR, a 2.15% higher SSIM, and a 50% lower LPIPS. Notably, our training time is significantly shorter than both baselines (see Sec. 4.3).

Scene	E2VID[54] + 3DGS[2]			EventNeRF[42]			Event3DGS (event-only)		
	PSNR ↑	SSIM ↑	LPIPS ↓	PSNR ↑	SSIM ↑	LPIPS ↓	PSNR ↑	SSIM ↑	LPIPS ↓
Drums	16.52	0.74	0.24	27.43	0.91	0.07	29.37	0.94	0.04
Lego	16.11	0.75	0.23	25.84	0.89	0.13	29.57	0.93	0.05
Chair	20.64	0.87	0.13	30.62	0.94	0.05	31.59	0.95	0.03
Ficus	23.33	0.88	0.12	31.94	0.94	0.05	32.47	0.95	0.03
Mic	20.47	0.89	0.14	31.78	0.96	0.03	33.83	0.98	0.02
Hotdog	22.45	0.90	0.12	30.26	0.94	0.04	32.35	0.96	0.03
Materials	18.62	0.85	0.15	24.10	0.94	0.07	31.03	0.96	0.03
Average	19.73	0.84	0.16	28.85	0.93	0.06	<b>31.46</b>	<b>0.95</b>	<b>0.03</b>

Table 1: Quantitative comparison on synthetic event-sequences (event-only)

**Real Sequences** Given that the E2VID[54] + 3DGS[2] baseline performs poorly on forward-looking real-world data, we compare our method only with EventNeRF[42]. Table 4 shows that Event3DGS significantly outperforms EventNeRF[42] across all real scenes and metrics, achieving +3.23 dB higher PSNR, 46.4% higher SSIM, and 63.8% lower LPIPS on average. Additionally, our training time is considerably shorter than EventNeRF[42] (see Sec. 4.3).

	Scene	EventNeRF[42]			Event3DGS (event-only)		
		PSNR $\uparrow$	SSIM $\uparrow$	LPIPS $\downarrow$	PSNR $\uparrow$	SSIM $\uparrow$	LPIPS $\downarrow$
EventNeRF	Bike	21.1	0.39	0.58	23.06	0.71	0.26
	Computer	20.89	0.71	0.31	24.11	0.87	0.08
Ours	Drum	20.37	0.64	0.49	22.65	0.81	0.2
	Plant	16.59	0.3	0.56	22.53	0.8	0.13
	Shoes	25.35	0.78	0.39	28.08	0.89	0.17
	Average	20.86	0.56	0.47	<b>24.09</b>	<b>0.82</b>	<b>0.17</b>

Figure 3: Qualitative comparison in low-light scenes (event-only). Figure 4: Quantitative comparison on real world event-sequences (event-only)

## 4.2 Qualitative Evaluation

We evaluate the reconstructed structure and appearance by visualizing depth maps and renderings on 3 synthetic scenes and 3 real-world scenes. Fig. 5 shows that our method maintains sharper, more consistent structures and cleaner backgrounds compared to EventNeRF [42]. Event3DGS is able to capture detailed information of object edges and geometric discontinuities, such as ficus leaves (2<sup>nd</sup> row), drum racks (3<sup>rd</sup> row) and show laces (5<sup>th</sup> row). Our renderings also exhibit higher contrast and sharper details, particularly in highlights and reflections. For example, in the scene of soccer shoes, our method accurately represents the reflected lights with correct depth, while EventNeRF [42] fail to reconstruct these details. In the bike sample, EventNeRF fails to represent high-frequency details of the grass, whereas our method accurately reconstruct the grass geometry and preserves details in the background. Event3DGS also demonstrates robust reconstruction performance in low-light conditions. As shown in Fig. 3, our method learns sharper object details with fewer noisy artifacts.

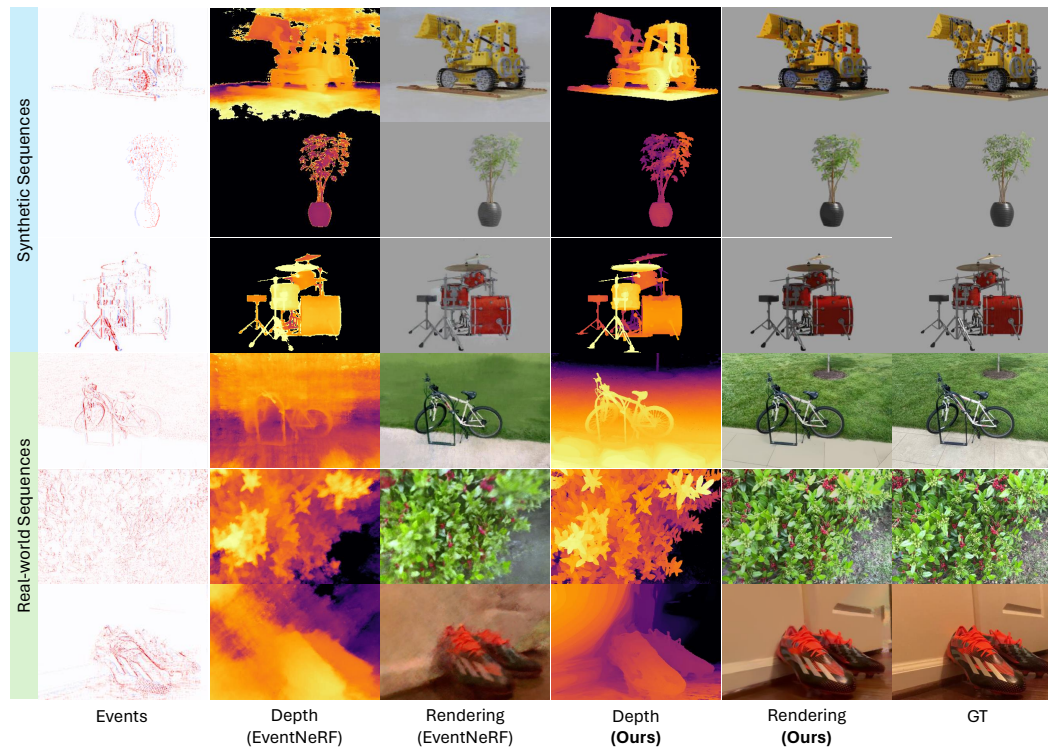


Figure 5: Qualitative comparison on synthetic and real-world sequences (event-only).

### 4.3 Ablation Studies and Efficiency Comparison

**Progressive Training** Fig. 6 shows an example of progressive training for improving reconstructing details. With the 3D structure of previous checkpoints, more gaussians are generated at under-reconstructed areas during the second round training via adaptive densification. Consequently, Event3DGS is able to progressively capture the subtle details (e.g. bicycle spokes and grasses) that are not accurately modeled during previous rounds.

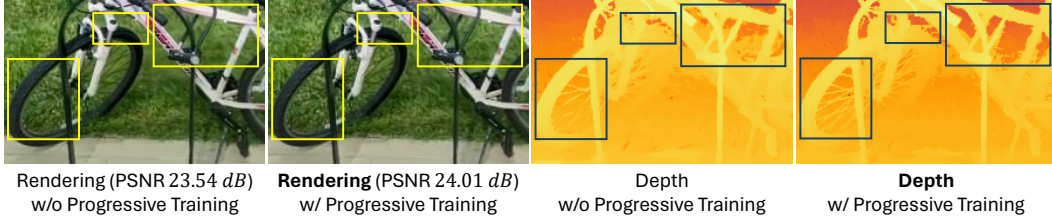


Figure 6: Ablation study of progressive training on the bike (event-only).

**Blur-aware Appearance Refinement** We finetune the appearance-related parameters on each synthetic scene adaptively with 50-300 iterations, and plot the average PSNR in Fig. 7. As shown, using up to 10 blurry RGB images already yields a noticeable enhancement in rendering quality.

**Model Efficiency.** As shown in Table. 8, Event3DGS reduce the training time of EventNeRF from 9 hours to less than 20 minutes while achieving 1000x higher FPS, enabling real-time rendering.

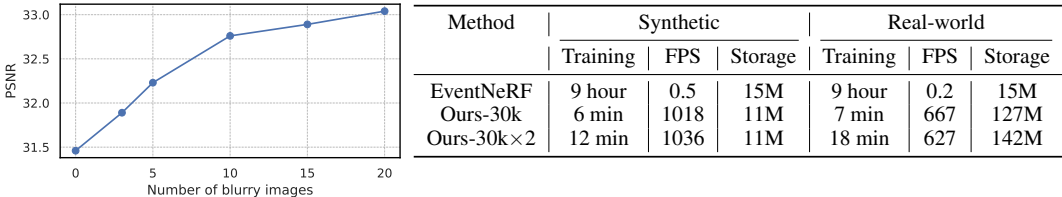


Figure 7: Ablations on number of blurry images. Figure 8: Efficiency comparison on synthetic and real-world sequences (event-only).

## 5 Conclusion

In this paper, we propose Event3DGS, a novel framework for learning a sharp explicit 3D representation solely from the raw stream of events. By integrating differential event supervision, sampling and progressive training strategies tailored to event data characteristics, Event3DGS achieves high-fidelity radiance field reconstruction under low-light and fast egomotion scenarios. Benefiting from the efficiency of 3D Gaussian Splatting, the proposed method reduce the training time of NeRF-based methods and allows real-time rendering. Furthermore, our parameter separable refinement strategy enhances the appearance via training on a minimal number of motion-blurred RGB images with negligible computational overhead. By incorporating the high temporal resolution of event cameras into 3DGS, the proposed method enables robots to conduct 3D mapping at higher execution speeds without sacrificing sharp details, offering practical solutions for deployment in real-world applications.

**Limitation and Future work.** The main limitation lays in the inherent characteristics of 3D Gaussian Splatting and event streams, including the bottleneck in memory inefficiency, and under-representation of texture details at plane surface (e.g. road under the bike, door behind the soccer shoes). Besides, accuracy pointcloud estimation from event streams is required for further improvement in reconstruction quality. We leave these challenges as future work.



## References

- [1] B. Mildenhall, P. P. Srinivasan, M. Tancik, J. T. Barron, R. Ramamoorthi, and R. Ng. Nerf: Representing scenes as neural radiance fields for view synthesis. In *ECCV*, 2020.
- [2] B. Kerbl, G. Kopanas, T. Leimkühler, and G. Drettakis. 3d gaussian splatting for real-time radiance field rendering. *ACM Transactions on Graphics*, 42(4), July 2023. URL <https://repo-sam.inria.fr/fungraph/3d-gaussian-splatting/>.
- [3] L. Ma, X. Li, J. Liao, Q. Zhang, X. Wang, J. Wang, and P. V. Sander. Deblur-nerf: Neural radiance fields from blurry images, 2022.
- [4] J. Oh, J. Chung, D. Lee, and K. M. Lee. Deblur-gs: Gaussian splatting for camera motion blur, 2024.
- [5] O. Seiskari, J. Ylilammi, V. Kaatrasalo, P. Rantalankila, M. Turkulainen, J. Kannala, E. Rahtu, and A. Solin. Gaussian splatting on the move: Blur and rolling shutter compensation for natural camera motion, 2024.
- [6] P. Wang, L. Zhao, R. Ma, and P. Liu. Bad-nerf: Bundle adjusted deblur neural radiance fields, 2023.
- [7] L. Zhao, P. Wang, and P. Liu. Bad-gaussians: Bundle adjusted deblur gaussian splatting, 2024.
- [8] C. Wenbo and L. Ligang. Deblur-gs: 3d gaussian splatting from camera motion blurred images. *Proc. ACM Comput. Graph. Interact. Tech. (Proceedings of I3D 2024)*, 7(1), 2024. doi:10.1145/3651301. URL <http://doi.acm.org/10.1145/3651301>.
- [9] Y. Hu, S.-C. Liu, and T. Delbruck. v2e: From video frames to realistic dvs events, 2021.
- [10] P. E. Debevec, C. J. Taylor, and J. Malik. Modeling and rendering architecture from photographs: A hybrid geometry-and image-based approach. In *Seminal Graphics Papers: Pushing the Boundaries, Volume 2*, pages 465–474. 2023.
- [11] A. Geiger, J. Ziegler, and C. Stiller. Stereoscan: Dense 3d reconstruction in real-time. In *2011 IEEE intelligent vehicles symposium (IV)*, pages 963–968. Ieee, 2011.
- [12] V. Sitzmann, M. Zollhöfer, and G. Wetzstein. Scene representation networks: Continuous 3d-structure-aware neural scene representations. *Advances in Neural Information Processing Systems*, 32, 2019.
- [13] Z. Ma and S. Liu. A review of 3d reconstruction techniques in civil engineering and their applications. *Advanced Engineering Informatics*, 37:163–174, 2018.
- [14] M. Adamkiewicz, T. Chen, A. Caccavale, R. Gardner, P. Culbertson, J. Bohg, and M. Schwager. Vision-only robot navigation in a neural radiance world. *IEEE Robotics and Automation Letters*, 7(2):4606–4613, 2022.
- [15] F. Bruno, S. Bruno, G. De Sensi, M.-L. Luchi, S. Mancuso, and M. Muzzupappa. From 3d reconstruction to virtual reality: A complete methodology for digital archaeological exhibition. *Journal of Cultural Heritage*, 11(1):42–49, 2010.
- [16] K. Zhang, G. Riegler, N. Snavely, and V. Koltun. Nerf++: Analyzing and improving neural radiance fields. *arXiv preprint arXiv:2010.07492*, 2020.
- [17] J. T. Barron, B. Mildenhall, M. Tancik, P. Hedman, R. Martin-Brualla, and P. P. Srinivasan. Mip-nerf: A multiscale representation for anti-aliasing neural radiance fields. In *Proceedings of the IEEE/CVF International Conference on Computer Vision*, pages 5855–5864, 2021.

- [18] J. T. Barron, B. Mildenhall, D. Verbin, P. P. Srinivasan, and P. Hedman. Mip-nerf 360: Unbounded anti-aliased neural radiance fields. In *Proceedings of the IEEE/CVF Conference on Computer Vision and Pattern Recognition*, pages 5470–5479, 2022.
- [19] R. Martin-Brualla, N. Radwan, M. S. Sajjadi, J. T. Barron, A. Dosovitskiy, and D. Duckworth. Nerf in the wild: Neural radiance fields for unconstrained photo collections. In *Proceedings of the IEEE/CVF Conference on Computer Vision and Pattern Recognition*, pages 7210–7219, 2021.
- [20] M. Tancik, V. Casser, X. Yan, S. Pradhan, B. Mildenhall, P. P. Srinivasan, J. T. Barron, and H. Kretschmar. Block-nerf: Scalable large scene neural view synthesis. In *Proceedings of the IEEE/CVF Conference on Computer Vision and Pattern Recognition*, pages 8248–8258, 2022.
- [21] P. Wang, L. Liu, Y. Liu, C. Theobalt, T. Komura, and W. Wang. Neus: Learning neural implicit surfaces by volume rendering for multi-view reconstruction. *arXiv preprint arXiv:2106.10689*, 2021.
- [22] Q. Xu, Z. Xu, J. Philip, S. Bi, Z. Shu, K. Sunkavalli, and U. Neumann. Point-nerf: Point-based neural radiance fields. In *Proceedings of the IEEE/CVF conference on computer vision and pattern recognition*, pages 5438–5448, 2022.
- [23] A. Chen, Z. Xu, A. Geiger, J. Yu, and H. Su. Tensorf: Tensorial radiance fields. In *European Conference on Computer Vision*, pages 333–350. Springer, 2022.
- [24] A. Yu, S. Fridovich-Keil, M. Tancik, Q. Chen, B. Recht, and A. Kanazawa. Plenoxels: Radiance fields without neural networks. *arXiv preprint arXiv:2112.05131*, 2(3):6, 2021.
- [25] C. Sun, M. Sun, and H.-T. Chen. Direct voxel grid optimization: Super-fast convergence for radiance fields reconstruction. In *Proceedings of the IEEE/CVF Conference on Computer Vision and Pattern Recognition*, pages 5459–5469, 2022.
- [26] T. Müller, A. Evans, C. Schied, and A. Keller. Instant neural graphics primitives with a multiresolution hash encoding. *ACM transactions on graphics (TOG)*, 41(4):1–15, 2022.
- [27] H. Matsuki, R. Murai, P. H. Kelly, and A. J. Davison. Gaussian splatting slam. *arXiv preprint arXiv:2312.06741*, 2023.
- [28] C. Yan, D. Qu, D. Wang, D. Xu, Z. Wang, B. Zhao, and X. Li. Gs-slam: Dense visual slam with 3d gaussian splatting. *arXiv preprint arXiv:2311.11700*, 2023.
- [29] Z. Yang, H. Yang, Z. Pan, X. Zhu, and L. Zhang. Real-time photorealistic dynamic scene representation and rendering with 4d gaussian splatting. *arXiv preprint arXiv:2310.10642*, 2023.
- [30] G. Wu, T. Yi, J. Fang, L. Xie, X. Zhang, W. Wei, W. Liu, Q. Tian, and X. Wang. 4d gaussian splatting for real-time dynamic scene rendering. *arXiv preprint arXiv:2310.08528*, 2023.
- [31] Y. Chen, Z. Chen, C. Zhang, F. Wang, X. Yang, Y. Wang, Z. Cai, L. Yang, H. Liu, and G. Lin. Gaussianeditor: Swift and controllable 3d editing with gaussian splatting. *arXiv preprint arXiv:2311.14521*, 2023.
- [32] M. Ye, M. Danelljan, F. Yu, and L. Ke. Gaussian grouping: Segment and edit anything in 3d scenes. *arXiv preprint arXiv:2312.00732*, 2023.
- [33] A. Baudron, Z. W. Wang, O. Cossairt, and A. K. Katsaggelos. E3d: Event-based 3d shape reconstruction, 2020.
- [34] M. Muglikar, G. Gallego, and D. Scaramuzza. Esl: Event-based structured light. In *2021 International Conference on 3D Vision (3DV)*, pages 1165–1174. IEEE, 2021.

- [35] Z. Wang, K. Chaney, and K. Daniilidis. Evac3d: From event-based apparent contours to 3d models via continuous visual hulls. In *European conference on computer vision*, pages 284–299. Springer, 2022.
- [36] K. Xiao, G. Wang, Y. Chen, J. Nan, and Y. Xie. Event-based dense reconstruction pipeline. In *2022 6th International Conference on Robotics and Automation Sciences (ICRAS)*, pages 172–177. IEEE, 2022.
- [37] A. Z. Zhu, L. Yuan, K. Chaney, and K. Daniilidis. Unsupervised event-based learning of optical flow, depth, and egomotion. In *Proceedings of the IEEE/CVF Conference on Computer Vision and Pattern Recognition*, pages 989–997, 2019.
- [38] W. Chamorro, J. Sola, and J. Andrade-Cetto. Event-based line slam in real-time. *IEEE Robotics and Automation Letters*, 7(3):8146–8153, 2022.
- [39] A. Mitrokhin, C. Ye, C. Fermüller, Y. Aloimonos, and T. Delbruck. Ev-imo: Motion segmentation dataset and learning pipeline for event cameras. In *IEEE/RSJ International Conference on Intelligent Robots and Systems (IROS)*, 2019.
- [40] C. Ye, A. Mitrokhin, C. Fermüller, J. A. Yorke, and Y. Aloimonos. Unsupervised learning of dense optical flow, depth and egomotion with event-based sensors. In *IEEE/RSJ International Conference on Intelligent Robots and Systems (IROS)*, pages 5831–5838, 2020.
- [41] I. Hwang, J. Kim, and Y. M. Kim. Ev-nerf: Event based neural radiance field. In *Proceedings of the IEEE/CVF Winter Conference on Applications of Computer Vision (WACV)*, pages 837–847, January 2023.
- [42] V. Rudnev, M. Elgharib, C. Theobalt, and V. Golyanik. Eventnerf: Neural radiance fields from a single colour event camera. In *Computer Vision and Pattern Recognition (CVPR)*, 2023.
- [43] A. Bhattacharya, R. Madaan, F. Cladera, S. Vemprala, R. Bonatti, K. Daniilidis, A. Kapoor, V. Kumar, N. Matni, and J. K. Gupta. Evidnerf: Reconstructing event data with dynamic neural radiance fields. In *Proceedings of the IEEE/CVF Winter Conference on Applications of Computer Vision (WACV)*, pages 5846–5855, January 2024.
- [44] Q. Ma, D. P. Paudel, A. Chhatkuli, and L. Van Gool. Deformable neural radiance fields using rgb and event cameras. In *Proceedings of the IEEE/CVF International Conference on Computer Vision*, pages 3590–3600, 2023.
- [45] Y. Qi, L. Zhu, Y. Zhang, and J. Li. E2nerf: Event enhanced neural radiance fields from blurry images. In *2023 IEEE/CVF International Conference on Computer Vision (ICCV)*, pages 13208–13218, Los Alamitos, CA, USA, oct 2023. IEEE Computer Society. doi: 10.1109/ICCV51070.2023.01219. URL <https://doi.ieeecomputersociety.org/10.1109/ICCV51070.2023.01219>.
- [46] M. Cannici and D. Scaramuzza. Mitigating motion blur in neural radiance fields with events and frames, 2024.
- [47] D. Weikersdorfer, R. Hoffmann, and J. Conradt. Simultaneous localization and mapping for event-based vision systems. In *Proceedings of the 9th international conference on Computer Vision Systems*, pages 133–142, 2013.
- [48] S. Klenk, L. Koestler, D. Scaramuzza, and D. Cremers. E-nerf: Neural radiance fields from a moving event camera. *IEEE Robotics and Automation Letters*, 2023.
- [49] W. F. Low and G. H. Lee. Robust e-nerf: Nerf from sparse & noisy events under non-uniform motion. In *Proceedings of the IEEE/CVF International Conference on Computer Vision*, pages 18335–18346, 2023.

- [50] Z. Wang, A. Bovik, H. Sheikh, and E. Simoncelli. Image quality assessment: from error visibility to structural similarity. *IEEE Transactions on Image Processing*, 13(4):600–612, 2004. doi:10.1109/TIP.2003.819861.
- [51] Y. Fu, S. Liu, A. Kulkarni, J. Kautz, A. A. Efros, and X. Wang. Colmap-free 3d gaussian splatting. *arXiv preprint arXiv:2312.07504*, 2023.
- [52] O. Keleş, M. A. Yılmaz, A. M. Tekalp, C. Korkmaz, and Z. Dogan. On the computation of psnr for a set of images or video, 2021.
- [53] R. Zhang, P. Isola, A. A. Efros, E. Shechtman, and O. Wang. The unreasonable effectiveness of deep features as a perceptual metric, 2018.
- [54] H. Rebecq, R. Ranftl, V. Koltun, and D. Scaramuzza. Events-to-video: Bringing modern computer vision to event cameras. *IEEE Conf. Comput. Vis. Pattern Recog. (CVPR)*, 2019.